12th AIAA/CEAS Aeroacoustics Conference (27th AIAA Aeroacoustics Conference), 8-10 May 2006, Boston

Sound Transmission in Strongly-Curved Slowly-Varying Cylindrical and Annular Lined Ducts with Flow

E.J. Brambley* N. Peake†

In this paper we consider the propagation of acoustic waves along a curved hollow or annular duct with lined walls. The curvature of the duct centreline and the wall radii vary slowly along the duct, allowing application of an asymptotic multiple scales analysis. This generalises Rienstra's analysis of a straight duct of varying cross-sectional radius. The result of the analysis is that the modal wavenumbers and mode shapes are determined locally as modes of a torus with the same local curvature, while the amplitude of the modes evolves as the mode propagates along the duct. The duct modes are found numerically at each axial location using a pseudo-spectral method. Unlike the case of a straight duct, there is a fundamental asymmetry between upstream and downstream propagating modes, with some mode shapes tending to be concentrated on either the inside or outside of the bend depending on the direction of propagation. The interaction between the presence of wall lining and curvature is investigated in particular; for instance, in a representative case it is found that the curvature causes the first few acoustic modes to be more heavily damped by the duct boundary than would be expected for a straight duct. Analytical progress can be made in the limit of very high mode order, in which case well-known 'whispering gallery' modes, localised close to the wall, can be identified.

I. Introduction

The propagation of acoustic waves along curved pipes has attracted much attention, with a wide range of applications. One application, which is the motivation for the research described in the current paper, is to the prediction of unsteady flow along the sort of convoluted intakes often found on the engines of military aircraft. One issue here might be the behaviour of sound generated by the fan as it propagates upstream, or alternatively at very large amplitudes the propagation of surge events.

A selection of previous work will be mentioned here. Keefe & Benade[1] used ideas of impedance matching to study the propagation of very long waves along a curved pipe. Pagneux and co-workers have developed mode-matching techniques to describe propagation in various sorts of curved ducts with zero mean flow,[2–5] and have also studied sound attenuation round a lined bend.[6] More analytically-based studies have tended to use specific limits, including slender curved ducts[7] and weakly curved ducts in two[8] and three dimensions.[9] In a different direction, Rienstra[10] derived a uniformly-valid approximation for the unsteady field in a straight duct with circular cross-section carrying mean flow which varies slowly in the axial direction. Rienstra's approach has been validated against finite element computations.[11] This work has been extended in a number of ways; for instance to the case of arbitrary cross-section,[12] swirling mean flow,[13] and to a uniform description of modal cut-off.[14] However, all of this has been for straight ducts, and the aim in the current paper is therefore to present an extension of Rienstra's analysis to the case of a curved duct with mean flow.

The paper is organised as follows. In section II we show how to write down the steady potential flow through a curved duct. In section III we describe the solution for the unsteady flow; as a mode propagates along the duct it is distorted, and the description of this process involves first the determination of the local axial wavenumber and mode shape and second the determination of the slowly-varying amplitude. This local

*PhD Student, DAMTP, University of Cambridge, Wilberforce Rd. Cambridge CB3 0WA, UK, AIAA Member.

†Professor of Applied Mathematics, DAMTP, University of Cambridge, Wilberforce Rd. Cambridge CB3 0WA, UK, AIAA Member.

eigenproblem must be solved numerically, and our pseudo-spectral method for doing this, together with error control and validation, is described in section IV. Results are presented in section V, while in section VI the way in which modes can transition from cuton to cutoff is considered. In section VII some initial results using ray theory to describe high-order duct modes are presented.

II. Steady flow

We consider a duct whose centreline possesses nonzero curvature but zero torsion (i.e. it lies in a plane). The duct is hollow or annular, and has a circular cross-section in planes normal to the centreline. Far upstream the duct is assumed to be straight and of uniform outer radius l^* (* denotes dimensional variables), and the radii of the outer (and inner) walls and the centreline curvature then vary slowly along the duct. Specifically, the radii and the curvature are taken to be functions of s^*/L^*, where s^* is the arc length along the centreline and L^* is their lengthscale of variation. We suppose that $l^*/L^* \equiv \epsilon \ll 1$. The duct carries a mean flow, which far upstream has uniform density D^*_∞, speed U^*_∞ and sound speed C^*_∞. In what follows speeds are non-dimensionalized by C^*_∞, densities by D^*_∞, distances by l^*, times by l^*/C^*_∞, and pressures by $(C^*_\infty)^2 D^*_\infty$. We introduce the duct-centred coordinate system (s, r, θ), where r, θ are polar coordinates in planes normal to the duct centreline, and s is the arc-length along the centreline with $s = -\infty$ corresponding to far upstream. The duct inner and outer radii are $a_{1,2}(S)$ and the centreline curvature is $\kappa(S)$, where $S = \epsilon s$ is the slow coordinate over which the duct geometry varies.

The steady velocity in the duct is given by $\boldsymbol{U} = U\boldsymbol{e_s} + V\boldsymbol{e_r} + W\boldsymbol{e_\theta}$, and it is assumed that all steady flow variables vary slowly down the duct. We assume an inviscid irrotational perfect gas, and it can then be shown that the mean density and velocity take the form

$$D = D_0 + O(\varepsilon^2), \qquad U = U_0 + O(\varepsilon^2), \qquad V = \varepsilon V_1 + O(\varepsilon^3), \qquad W = \varepsilon W_1 + O(\varepsilon^3),$$

where

$$U_0(S, r, \theta) = \frac{U_\dagger(S)}{h_s}, \qquad\qquad D_0 = \left[(\gamma - 1)\left(H - \frac{1}{2}{U_0}^2\right)\right]^{1/\gamma - 1} .$$

Here $h_s = 1 - \kappa r \cos\theta$, γ is the ratio of specific heats and H is the constant enthalpy. The quantity $U_\dagger$ may be found by equating the mass flux at arc length S to that far upstream, to give the implicit equation

$$\int_0^{2\pi}\int_{a_1}^{a_2} U_0 D_0 r \,\mathrm{d}r \,\mathrm{d}\theta = \pi U_\infty (1 - a_1(-\infty)^2) .$$

It turns out that the value of the $O(\epsilon)$ radial velocity V_1 is only required on the walls, while the value of the $O(\epsilon)$ tangential velocity W_1 will not be required at all in the final answer for the unsteady flow. We suppose that the walls are hard for the purposes of determining the steady flow, so that

$$V_1(r, \theta, S) = \varepsilon \frac{1}{h_s}\frac{\mathrm{d}a_j}{\mathrm{d}S} U \qquad\qquad \text{at } r = a_j(S) \quad j = 1, 2 .$$

One duct geometry we shall consider in particular is the RAE 2129 Inlet Diffuser duct,[15] which is a much studied reference duct geometry. The duct geometry is defined in terms of the lateral offset of the centreline, y^*, from its position at the intake $s^* = 0$, with

$$y^*(s^*) = -\frac{h^*}{2}\left(1 - \cos\left(\frac{\pi s^*}{L^*}\right)\right) . \tag{1}$$

The lateral offset at the nominal fan face ($s^* = L^*$) is then h^*. The duct itself is hollow, with outer radius varying quartically between the inlet (radius l^*) and fan face (radius a^*_f) as

$$\frac{a^*(s^*) - l^*}{a^*_f - l^*} = 3\left(1 - \frac{s^*}{L^*}\right)^4 - 4\left(1 - \frac{s^*}{L^*}\right)^3 + 1 . \tag{2}$$

For the RAE 2129 duct, $L^*/l^* = 7.1$, $h^*/L^* = 0.3$ and $(a^*_f/l^*)^2 = 1.4$. For this choice we see that $\epsilon = 1/7.1$, for which it is reasonable to suppose that the small-ϵ asymptotics will work well. A cross-section along the duct centreline is shown in figure 1, along with the mean flow for a uniform inlet Mach number $U_\infty = 0.5$.

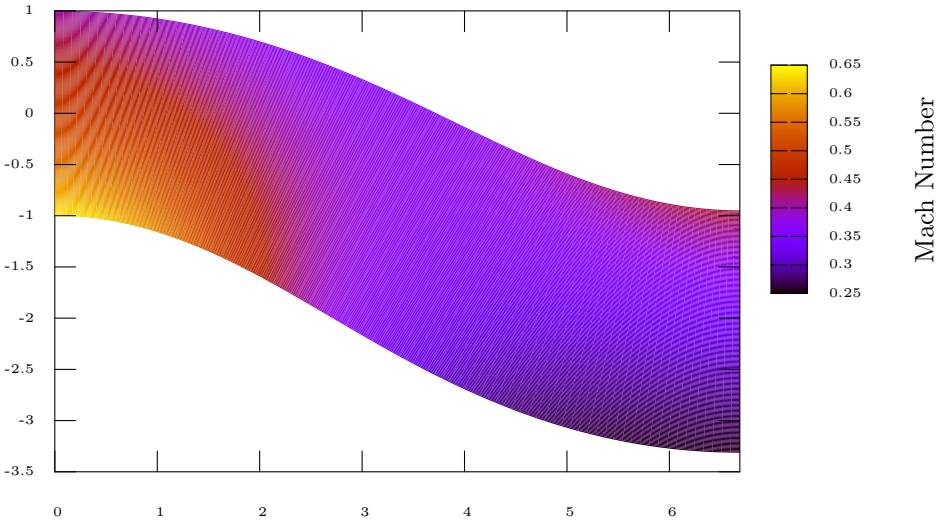

Figure 1. Mean flow in the RAE 2129 Inlet Diffuser. Uniform inlet Mach number from left of 0.5**.**

III. Unsteady flow

Consider a small time-dependent perturbation $(\boldsymbol{u}, \rho, p)$ to the mean flow $(\boldsymbol{U}, D, P)$. Introducing a scalar potential $\boldsymbol{u} = \boldsymbol{\nabla}\phi$, and neglecting vortical and entropic perturbations, Goldstein's equations[16] for the unsteady linearised flow reduce to

$$p = C^2\rho = -D\frac{\mathrm{D}\phi}{\mathrm{D}t}, \qquad \frac{\mathrm{D}}{\mathrm{D}t}\left(\frac{1}{C^2}\frac{\mathrm{D}\phi}{\mathrm{D}t}\right) - \frac{1}{D}\boldsymbol{\nabla}\cdot\left(D\boldsymbol{\nabla}\phi\right) = 0, \tag{3}$$

where $\mathrm{D}/\mathrm{D}t = \partial/\partial t + \boldsymbol{U}\cdot\boldsymbol{\nabla}$ is the convective derivative with respect to the mean flow. This equation is to be solved subject to the usual Myers[17] boundary condition for a lined duct, namely

$$-\mathrm{i}\omega\boldsymbol{\nabla}\phi.\boldsymbol{n} = \left\{\mathrm{i}\omega + \boldsymbol{U}.\boldsymbol{\nabla} - \boldsymbol{n}.[(\boldsymbol{n}.\boldsymbol{\nabla})\boldsymbol{U}]\right\}\frac{p}{Z_j} \quad \text{on } r = a_j(S) \text{ for } j = 1, 2\,, \tag{4}$$

where $Z_{1,2}(S)$ are the wall impedances and $\boldsymbol{n}$ is the corresponding wall normal pointing into the fluid.

In order to account for the slowly varying duct we follow Rienstra[10] and pose the multiple scales WKB ansatz (see for instance Hinch[18])

$$\phi = \left[A_0(S, r, \theta) + \epsilon A_1(S, r, \theta) + O(\epsilon^2)\right]\exp\left\{\mathrm{i}\omega t - \frac{\mathrm{i}}{\varepsilon}\int_{-\infty}^{S} k(S')\,dS'\right\}\,,$$

where ω is the fixed driving frequency. Taking just the $O(1)$ terms in (3) then leads to

$$\frac{1}{h_s D_0}\left[\frac{1}{r}\frac{\partial}{\partial r}\left(r h_s D_0\frac{\partial A_0}{\partial r}\right) + \frac{1}{r^2}\frac{\partial}{\partial\theta}\left(h_s D_0\frac{\partial A_0}{\partial\theta}\right)\right] + \left(\frac{\Lambda^2}{{C_0}^2} - \frac{k^2}{{h_s}^2}\right)A_0 = 0\,, \tag{5}$$

where $\Lambda = \omega - kU_0/h_s$. The $O(1)$ boundary condition is

$$\pm\frac{\partial A_0}{\partial r} = \frac{\mathrm{i}}{\omega}\left(\omega - \frac{kU}{h_s}\right)^2\frac{A_0 D_0}{Z_j} \quad \text{on } r = a_j(S) \text{ for } j = 1, 2\,, \tag{6}$$

where $Z_{1,2}$ are the impedances on the inner and outer walls respectively and $\pm$ refer to the inner and the outer walls respectively. For hard walls (6) becomes simply $\partial A_0/\partial r = 0$. One crucial difference here from the case of a straight circular duct is the highly nontrivial dependence of A_0 on θ. When $\kappa = 0$ equations (5) &

(6) can be solved using separation of variables to yield a well-known solution proportional to $\exp(-\mathrm{i}m\theta)$ for integer m. But when $\kappa \neq 0$ equation (5) is no longer separable and one must resort to the sort of numerical solution procedure described in the next section.

Equations (5) & (6) are now solved numerically to determine the axial wavenumber $k(S)$ and the corresponding wave function $\hat{A}_0(S,r,\theta)$. Details are given in the next section. We then have that

$$A_0(S,r,\theta) = N(S)\hat{A}_0(S,r,\theta)\ , \tag{7}$$

where we take the eigenfunction $\hat{A}_0(S,r,\theta)$ to be normalised as

$$\int_0^{2\pi}\int_{a_1}^{a_2} \frac{D_0 U_0 \omega}{{C_0}^2} {\hat{A}_0}^2 r\,\mathrm{d}r\,\mathrm{d}\theta = 1.$$

The unknown amplitude $N(S)$ must be determined from the solvability condition obtained using the $O(\epsilon)$ terms from (3) and (4). After a great deal of algebra we arrive at the requirement that the quantity

$$\left\{ F(S) - \mathrm{i}\left[\int_0^{2\pi} \frac{UD^2 r}{\omega Z_2}\left(\omega - \frac{kU}{h_s}\right){\hat{A}_0}^2 \mathrm{d}\theta\right]_{r=a_2} - \mathrm{i}\left[\int_0^{2\pi} \frac{UD^2 r}{\omega Z_1}\left(\omega - \frac{kU}{h_s}\right){\hat{A}_0}^2 \mathrm{d}\theta\right]_{r=a_1} \right\} N(S)^2 \tag{8}$$

is independent of S, where

$$F(S) = \int_0^{2\pi}\int_{a_1}^{a_2} D_0 {\hat{A}_0}^2 \left[\frac{\omega U_0}{{C_0}^2} + \frac{k}{h_s}\left(1 - \frac{{U_0}^2}{{C_0}^2}\right)\right] r\,\mathrm{d}r\,\mathrm{d}\theta\ .$$

In the case of rigid walls (8) reduces to the condition that $F(S)N(S)^2$ is constant along the duct, which for cut-on modes can be interpreted as conservation of energy. For finite impedance, the second and third terms in (8) are associated with absorption by the slowly-varying outer and inner duct walls (note these terms are surface integrals).

Putting all this together, we now have the leading-order solution (7) for the unsteady flow, in which the local axial wavenumber and modeshape are determined by numerical solution of (5) & (6) and the slowly varying amplitude is then given by (8).

IV. Numerical solution

A. Eigenvalue problem

Our first task is to solve the leading-order eigenvalue problem so as to determine the local axial wavenumber k and corresponding eigenfunctions as functions of the slow arc length S. The leading-order equation for A_0 and k is recast as the generalised eigenvalue problem

$$\begin{pmatrix} \mathcal{L} & 0 \\ 0 & 1 \end{pmatrix} \begin{pmatrix} A_0 \\ B_0 \end{pmatrix} = k \begin{pmatrix} \dfrac{2\omega U_0}{h_s {C_0}^2} & \dfrac{1}{{h_s}^2}\left(1 - \dfrac{{U_0}^2}{{C_0}^2}\right) \\ 1 & 0 \end{pmatrix} \begin{pmatrix} A_0 \\ B_0 \end{pmatrix}, \tag{9}$$

where

$$\mathcal{L}A_0 = \frac{1}{h_s D_0}\left[\frac{1}{r}\frac{\partial}{\partial r}\left(r h_s D_0 \frac{\partial A_0}{\partial r}\right) + \frac{1}{r^2}\frac{\partial}{\partial \theta}\left(h_s D_0 \frac{\partial A_0}{\partial \theta}\right)\right] + \frac{\omega^2}{{C_0}^2} A_0,$$

subject to the boundary conditions

$$\pm\frac{\partial A_0}{\partial r} - \frac{\mathrm{i}\omega D_0}{Z_{1,2}} A_0 = -\frac{2\mathrm{i}U_0 D_0}{h_s Z_{1,2}} B_0 + k\frac{\mathrm{i}D_0 {U_0}^2}{{h_s}^2 \omega Z_{1,2}} B_0,$$

where the positive sign is taken for the inner boundary (if one is present), and the negative sign for the outer boundary. This problem must be solved numerically, and we use a pseudo-spectral method with Chebyshev polynomials as the radial basis[19] and with trigonometric polynomials in the azimuthal direction.

Let n_r and n_θ be the required number of collocation points in the radial and azimuthal directions respectively (note that n_θ must be odd, since all trigonometric polynomials have an odd number of degrees of freedom). For an annular duct, the interval $r \in [a_1, a_2]$ is mapped linearly onto the interval $\xi(r) \in [-1, 1]$, such that $\xi(a_1) = 1$ (for a hollow duct, a_1 is replaced by a small nonzero δ). The Chebyshev polynomials are defined on $[-1, 1]$ by $T_j(\cos\theta) = \cos(j\theta)$, with collocation points

$$\xi_j = \cos^{-1}\left(\frac{j\pi}{n_r - 1}\right) \qquad\qquad j = 0, \ldots, n_r - 1.$$

The azimuthal collocation points are at $\theta_\ell = 2\ell\pi/n_\theta$, $\ell = 0, 1, ..., n_\theta - 1$.

Our system is now discretized for an annular duct by requiring the boundary conditions to be satisfied at collocation points $(0, \ell)$ and $(n_r - 1, \ell)$, and equation (9) to be satisfied at collocation points (j, ℓ) for $\ell = 0, \ldots, n_\theta - 1$ and $j = 1, \ldots, n_r - 2$. For a hollow duct, equation (9) is also required to be satisfied at collocation points $(0, \ell)$, and the inner boundary condition is dropped. After a series of manipulations, which include representation of the r and θ derivatives using standard spectral differentiation matrices, we arrive at a generalised eigenvalue problem which is now $2n_\theta(n_r - d)$ square ($d = 1, 2$ for hollow and annular ducts respectively). This was solved using the QZ algorithm, as implemented in the LAPACK[a] library routine `ZGGEV`.

In order to avoid spurious eigenvalues, two filtering processes were used. The first, based loosely on that described by Boyd[20] (chapter 7, p137–139), attempts to remove any eigenvectors who's eigenvalues vary significantly with the discretization used. Let the numerical eigenvalues of the given problem be λ_j, and the numerical eigenvalues of a reference problem, generated with slightly different values of n_r and n_θ, be μ_ℓ. Define the *continuity* of an eigenvalue λ_m to be

$$\frac{\inf_\ell |\lambda_m - \mu_\ell|}{\sqrt{({d_1}^2 + {d_2}^2)/2}},$$

where d_i is the distance between λ_m and the i^{th} nearest λ_j with $j \neq m$. The normalisation by the distance to the next closest eigenvalue is to ensure the continuity is scale free. The reason for the averaging over d_1 and d_2 is to deal with doubly-degenerate eigenvalues. A small continuity indicates the eigenvalue is stable under small changes to the discretization, and hence that it is a good candidate for a physical eigenvalue.

The second filtering attempts to remove eigenfunctions for which n_r or n_θ are not large enough to properly resolve. In order to do this, the solutions is decomposed into its spectral representation

$$\tilde{f}(r, \theta) = \sum_{j=0}^{n_r - 1} \sum_{\ell = \frac{n_\theta - 1}{2}}^{\frac{n_\theta - 1}{2}} a_{j\ell} T_j\big(\xi(r)\big) \mathrm{e}^{\mathrm{i}\ell\theta},$$

by performing a Discrete Cosine Transform (DCT) in the r direction, and a Fast Fourier Transform (FFT) in the θ direction, implemented using the FFTW[b] library's `dft_2d` transform. Figure 2 shows the spectral coefficients for a well resolved numerical eigenfunction, for which the outlying spectral coefficients are of the order of the machine precision (2×10^{-16}). Motivated by this figure, the boundary within which a well resolved eigenfunction should have small spectral coefficients is defined as

$$\mathcal{B} = \left\{ (j, \ell) : \begin{array}{c} n_r - b_r \leq j < n_r \\ \text{or} \\ (n_\theta + 1)/2 - b_\theta \leq |\ell| < (n_\theta + 1)/2 \end{array} \right\}.$$

The *resolvedness* of an eigenfunction with spectral coefficients $a_{j\ell}$ is defined to be

$$\frac{\sup\limits_{(j,\ell) \in \mathcal{B}} |a_{j\ell}|}{\sup\limits_{\text{all } j,\ell} |a_{j\ell}|}.$$

Using $b_r = 2$ and $b_\theta = 4$, the eigenfunction of figure 2 has a resolvedness of 2.021×10^{-12}.

Numerically generated eigenvalues and eigenvectors that did not have a suitably small continuity or resolvedness were discarded.

[a] `http://www.netlib.org/lapack`
[b] `http://www.fftw.org`

B. Code validation

In the case of a straight duct with hard walls it is well known[10] that equation (5) can be solved analytically, with solutions in terms of Bessel's functions $A(r,\theta) = (P\mathrm{J}_m(\alpha r) + Q\mathrm{Y}_m(\alpha r))e^{-\mathrm{i}m\theta}$. Requiring a non-trivial solution satisfying the boundary conditions $\partial A/\partial r = 0$ yields the dispersion relation

$$\mathrm{J}_m{}'(\alpha a_1)\mathrm{Y}_m{}'(\alpha a_2) - \mathrm{J}_m{}'(\alpha a_2)\mathrm{Y}_m{}'(\alpha a_1) = 0 \,, \tag{10}$$

with solutions $\alpha = \alpha_{mn}$ for $n = 1, 2, \ldots$. Since Bessel's equation is self-adjoint, with weight function $w(r) = r$, and since the trigonometric polynomials are orthogonal, each of these solutions are orthogonal to one another with respect to the inner product

$$< \phi, \psi >= \int_0^{2\pi}\int_{a_1}^{a_2} \overline{\phi(r,\theta)}\psi(r,\theta) r \,\mathrm{d}r \,\mathrm{d}\theta,$$

where the overbar denotes complex conjugate. As a means of validation, the numerically generated solutions for a straight duct were compared with the analytic solutions. For eigenvalues, the measure of accuracy was taken to be the continuity defined in the previous subsection. For eigenfunctions, the numerical solutions were separated into a component in the direction of the analytic solution and an orthogonal component, with respect to the above inner product, and the error was taken to be the norm of the orthogonal component.

The numerical solutions were calculated at varying values of (n_r, n_θ) from $(21, 21)$ to $(41, 81)$. These were compared to all the analytic modes that passed the resolvedness test at the $(21, 21)$ resolution. Figure 3 shows the accuracy of the eigenvalues and eigenfunctions. Since the analytic modes have $\mathrm{e}^{-\mathrm{i}m\theta}$ dependence, which are also the azimuthal basis functions for the pseudo-spectral method, all analytic modes considered were well resolved in the azimuthal direction and so little variation was seen beyond $n_\theta = 21$. For small values of n_r some modes were not accurately resolved, explaining the initial plateau. For large values of n_r machine precision errors become apparent. In the intermediate region, an exponential decrease in error was seen, as is expected from a pseudo-spectral method. While the arithmetic mean error for all modes is plotted, similar results were obtained from taking the geometric mean and the maximum error.

V. Results

The numerics above were first applied to a hypothetical duct, with upstream conditions $U_\infty = 0.5$, $a_1 = 0.4$, $a_2 = 1.0$, $\gamma = 1.4$ and $\omega = 10$. The curvature of the duct was considered to vary slowly from $\kappa = 0$ upstream to $\kappa = 0.1$, at which point the wave modes were calculated.

The numerical eigenvalues for an annular duct with this geometry are shown in figure 4a,b. Figures 4c and 4d show examples of cross-sectional modal shapes. Both of these are upstream propagating modes, and the fundamental mode in figure 4c is seen to be localized in the inside of the bend. The downstream propagating modes have similar shapes, but are localized on the outside of the bend. Figures 4e and 4f show typical higher order modes, both of which are cutoff modes. These modal shapes are termed *bouncing ball* and *whispering gallery* type modes respectively, in light of the ray-tracing approximations in §VII.

One interesting feature of the spectrum is the diagonal vanes of eigenvalues occurring periodically across the usual line of cutoff modes in figure 4a and in close-up in figure 4b. This only seems to appear in the presence of both non-zero mean flow and non-zero curvature, and can perhaps be associated with the asymmetric mean flow and asymmetric mode shapes leading to slightly different Doppler shifts experienced by each mode. Similar results can also be seen for a hollow rather than annular duct cross-sections.

Figure 5a shows some eigenvalues for a curved ($\kappa = 0.1$), lined ($Z = 2 - \mathrm{i}$) hollow duct with mean flow ($U_\infty = 0.5$). The additional series of eigenvalues in the lower-half k-plane correspond to surface modes — see Rienstra[21] and Brambley & Peake.[22] Figure 5d shows how such a mode is strongly localised near the boundary, while figure 5c shows the upstream-propagating acoustic mode of the same order. This latter mode is termed a whispering gallery mode (see later), and while still being localised close to the outer boundary is noticeably more pervasive into the duct than the surface mode. At the other extreme is the bouncing-ball mode shown in figure 5b. These modes are similar to the high-order modes in a hard-wall duct, except that for the lined duct there is very little oscillation at the duct wall. Figures 5e and 5f show the fundamental duct modes, and illustrate the asymmetry between upstream- and downstream-propagating modes. The upstream-propagating mode is removed from the boundary, similar to a mode with a pressure-release boundary condition, while the curvature biases the mode slightly to the inside of the bend (the right

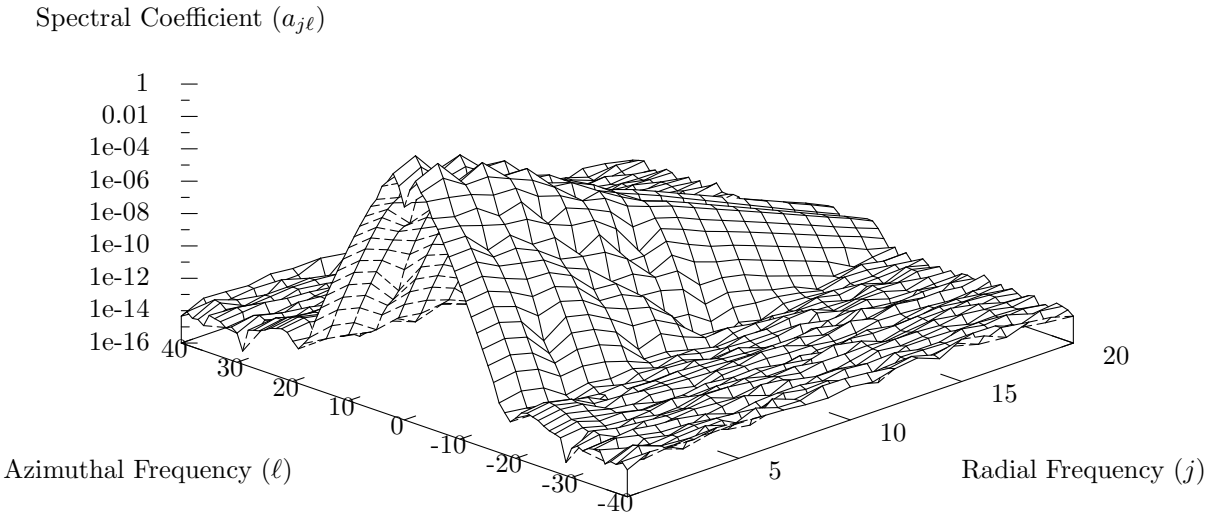

Figure 2. The spectral coefficients for a well resolved eigenfunction with eigenvalue $k = -17.77$. $U_\infty = 0.5$, $\kappa = 0.1$, $a_1 = 0.4$, $a_2 = 1.0$, $\gamma = 1.4$, $\omega = 10$, $n_r = 21$, $n_\theta = 81$.

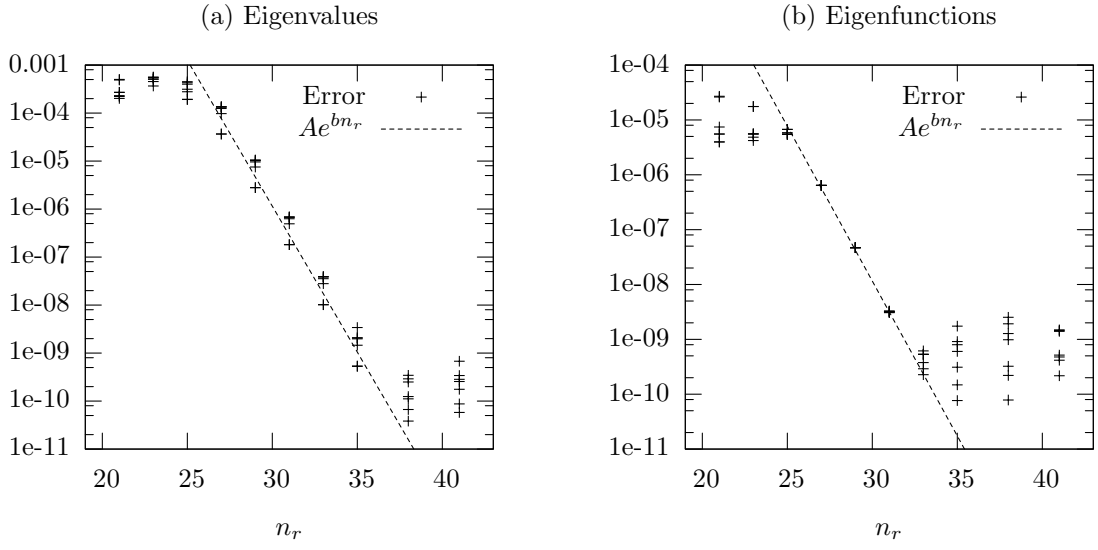

Figure 3. Mean numerical error. $U_\infty = 0.5$, $a_1 = 0.4$, and $a_2 = 1.0$. The line shown has slope (a) $b = -1.4$, (b) $b = -1.3$.

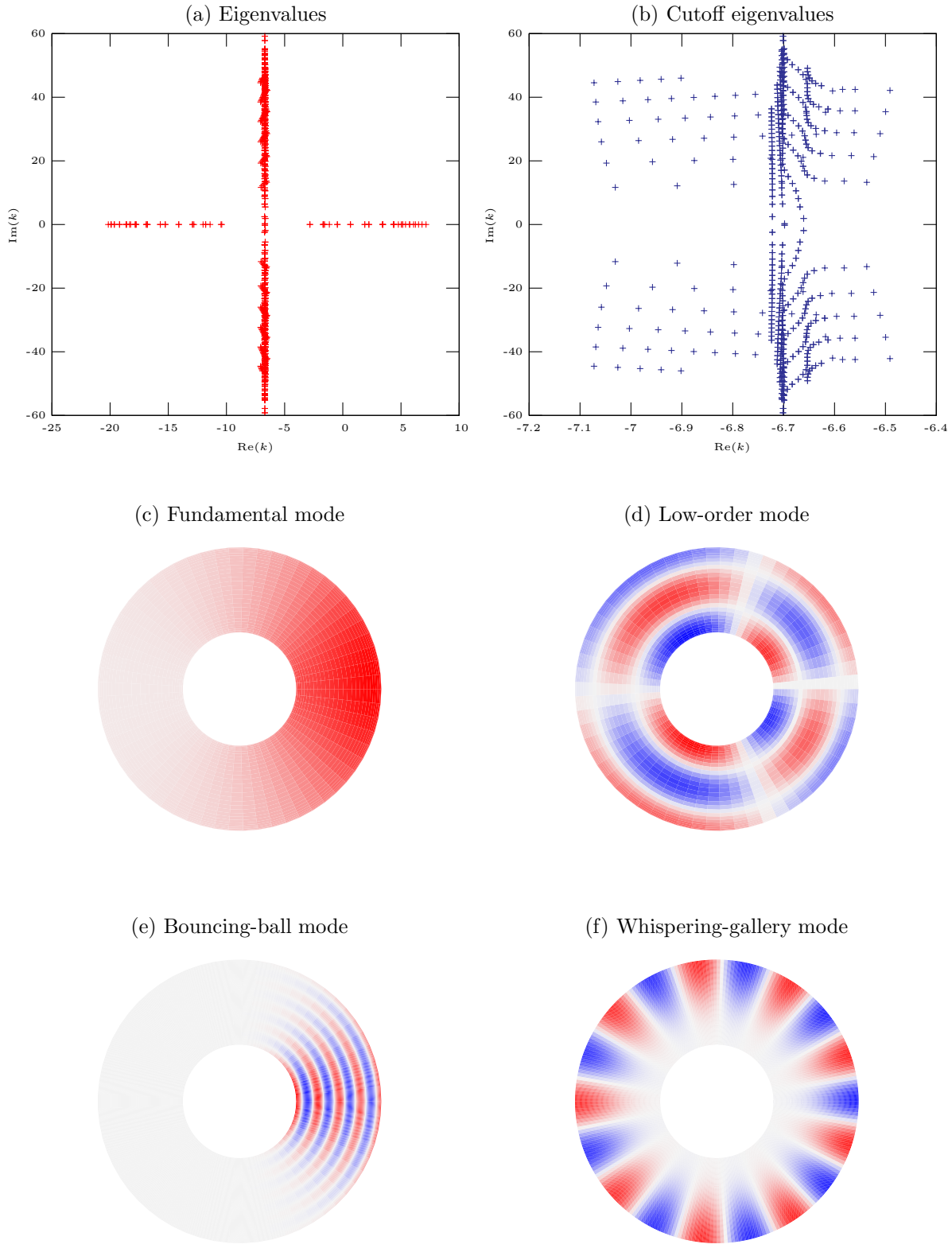

Figure 4. Results for a hard-walled annular duct, (b) being a close-up of the cut-off modes in (a). The modes in (c)–(f) are all downstream propagating, with the inside of the bend on the right. $U_\infty = 0.5$, $\omega = 10$, $a_1/a_2 = 0.4$, **and** $\kappa = 0.1$.

(a) Eigenvalues

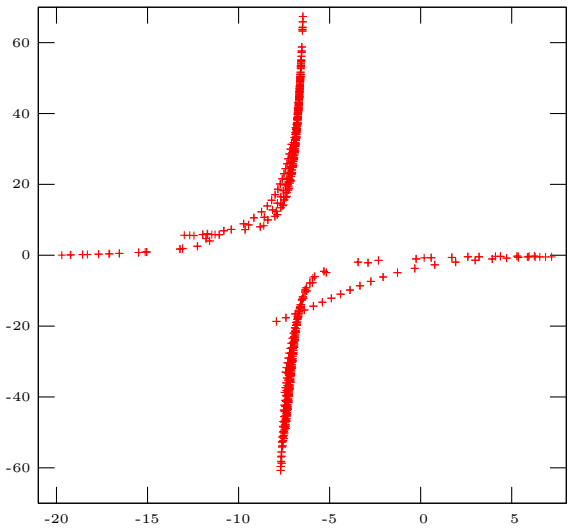

(b) A bouncing-ball mode

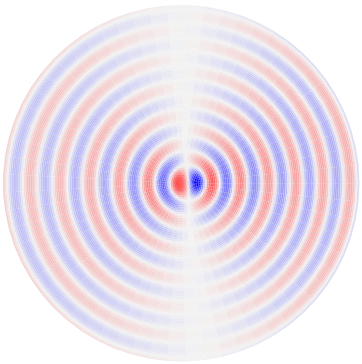

(c) A whispering-gallery mode

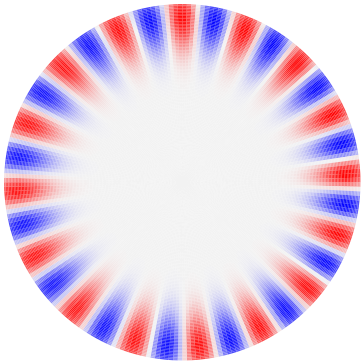

(d) A surface mode

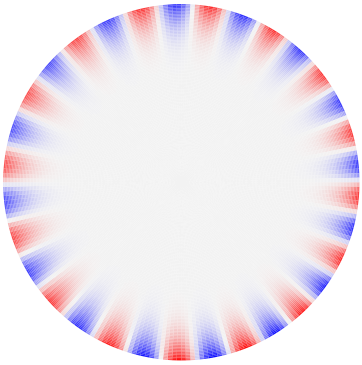

(e) The upstream fundamental mode

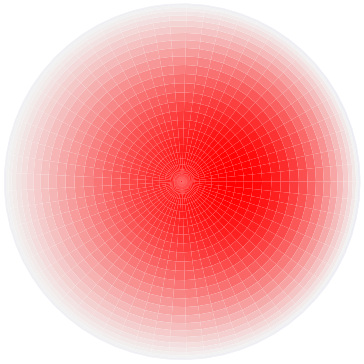

(f) The downstream fundamental mode

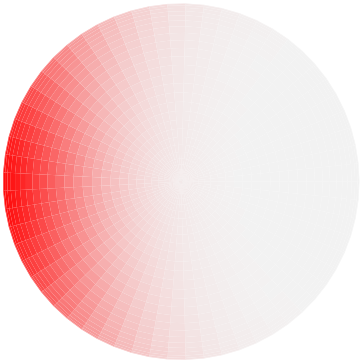

Figure 5. Results for a lined curved duct. $U_\infty = 0.5$, $\kappa = 0.1$, $Z = 2 - \mathrm{i}$, **and** $\omega = 10$.

hand side). The downstream-propagating mode, in contrast, is strongly localised to the outside of the bend, and is oscillating significantly on the duct boundary; it is very similar in form to a hard-wall duct mode.

Figures 6 & 7 shows how the axial wavenumbers k vary with the curvature κ. Note that due to the left-right asymmetry for $\kappa \neq 0$, two modes with $\kappa \neq 0$ merge into a single mode with $\kappa = 0$. As the curvature increases from zero, the first few downstream modes (figure 7) become more damped. In contrast, the surface modes (i.e. the lower branch in the right half plane) for $k \lesssim 5$ become less damped, while most of the well cutoff acoustic modes (i.e. the ones in the line parallel to the vertical in figure 5) maintain the same rate of decay, although their phase speed shifts slightly towards upstream.

Turning now to the RAE 2129 (hard-walled) duct described in section II, the cut-on eigenvalues (i.e. those with real axial eigenvalue k) are plotted against the position along the duct centreline in figure 8. As can be seen, many modes which are cut-on at the fan face ($s \approx 7$) will propagate all the way to the intake ($s = 0$). In figure 9 the amplitude of one such cut-on mode is plotted, and as can be seen in this case the amplitude varies rather little along the duct, with this high-order mode being concentrated close to the duct wall all the way along. As can be seen in figure 8, there are also in this case several duct modes which transition from cutoff to cuton within the duct, i.e. the sequence of real wavenumbers starting at the fan reaches a minimum value of s before turning round and moving back towards the fan (e.g. four around $s \approx 2$ etc). The transitions correspond to wave reflection by the changing geometry and flow, and will be described in detail in the next section. The cut-off transition confines these modes to the fan end of the duct. The amplitude of just one of the cutoff modes is shown in 10, indicating the standing-wave pattern formed by the mode and its reflection between the fan and the transition point. This suggests the possibility of acoustic resonance, in which acoustic modes are trapped upstream of the fan by the cut-off transition and are prevented from propagating downstream by the swirl in the rotor-stator gap - see Cooper & Peake.[23]

VI. Turning points and wave reflection

For a hard-walled duct the secularity condition (8) represents conservation of axial energy flux. Since a cuton mode has a non-zero energy flux and a cutoff mode has zero energy flux, it is to be expected that the secularity condition breaks down in the neighbourhood of a cuton–cutoff transition. The secularity condition (8) becomes singular when $F(S) \to 0$, a so-called *turning point*. Define

$$G(S) = \int_0^{2\pi} \int_{a_1}^{a_2} \frac{D_0}{h_s} \hat{A_0}^2 \left(1 - \frac{{U_0}^2}{{C_0}^2}\right) r \, \mathrm{d}r \, \mathrm{d}\theta,$$

so that $k = (F(S) - 1)/G(S)$. From previous studies on a straight duct,[10] we can expect that this transition occurs over a portion of the S axis of length $O(\epsilon^{2/3})$, and since $G(S)$ will vary little over this interval it follows that the change in k from real (cut-on) to complex (cut-off) is associated with a change of sign of $F(S)^2$. Figure 11 shows the variation in $F(S)^2$ for a mode in the RAE 2129 duct that undergoes a cuton–cutoff transition; in the neighbourhood of the cutoff region, $F(S)^2$ is seen to be a linear function of S, and goes through zero as the mode transitions from cuton to cutoff.

The singularity in the secularity condition (8) can be removed by inclusion of a second derivative term from higher order, so that the secularity condition becomes

$$\frac{\mathrm{d}}{\mathrm{d}S}\left(FN^2\right) + \mathrm{i}\varepsilon GN\frac{\mathrm{d}^2 N}{\mathrm{d}S^2} = 0. \tag{11}$$

Let the turning point be at S_0, so that $F(S_0 + \Delta S) = \sqrt{a\Delta S}$ for some a. In what follows an inbound downstream propagating mode is considered (exactly the same analysis can be applied to an upstream propagating mode, for example as in the RAE2129 duct), so that a is negative. By introducing the inner variable

$$x = \Delta S \varepsilon^{-2/3} G^{-2/3} a^{1/3},$$

(11) becomes

$$N'' + 2\mathrm{i}\sqrt{x}N' + \frac{\mathrm{i}N}{2\sqrt{x}} = 0,$$

with leading order solution

$$N = \left(A\mathrm{Ai}(-x) + B\mathrm{Bi}(-x)\right) \exp\left\{-\frac{2\mathrm{i}}{3}x^{3/2}\right\}.$$

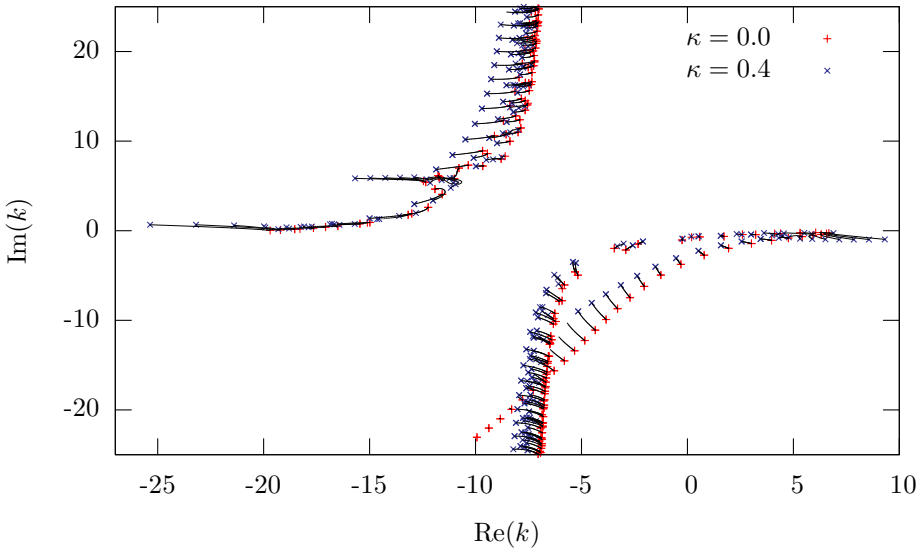

Figure 6. Graph showing the motion of eigenvalues due to varying the curvature from $\kappa = 0.0$ to $\kappa = 0.4$. $Z = 2 - \mathrm{i}$, $U_\infty = 0.5$, and $\omega = 10.0$.

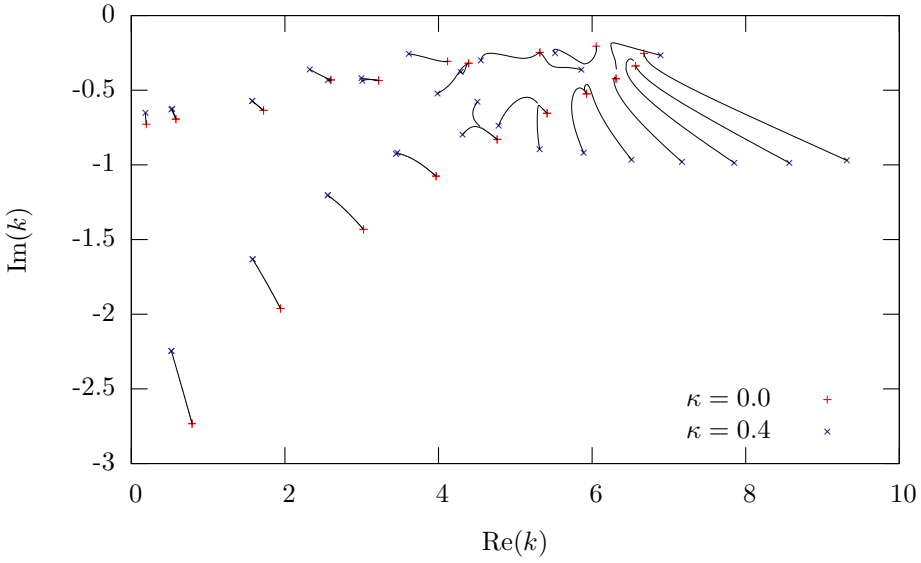

Figure 7. Close up of nearly cut-on modes in figure 6.

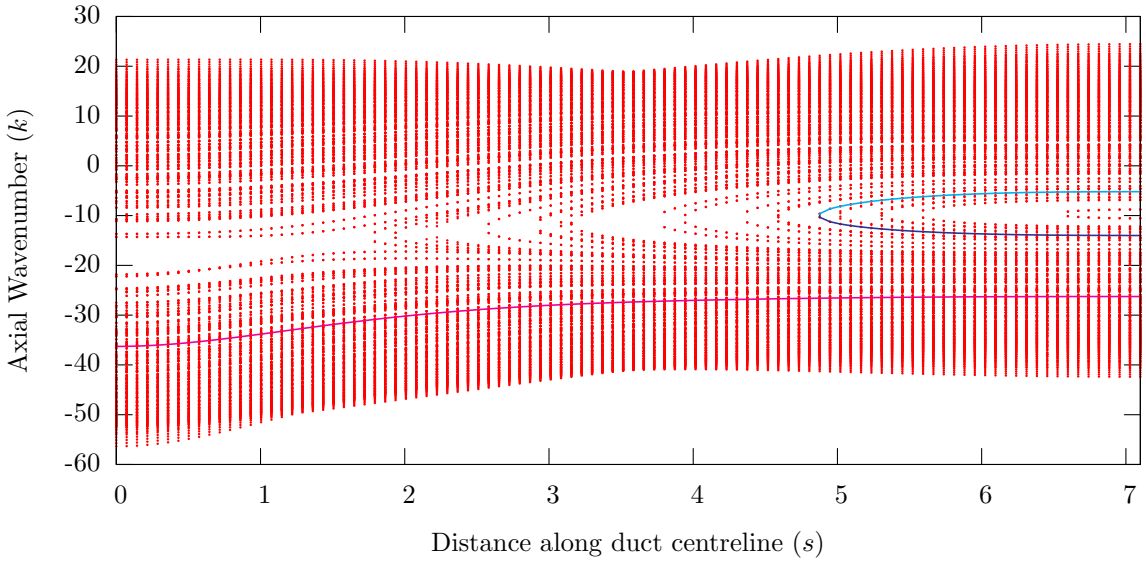

Figure 8. Real eigenvalues in the RAE 2129 Inlet Diffuser shown in figure 1, for $\omega = 26.2$, giving $a_2^* \omega^* / C_\infty^* = 31.0$ at the fan face ($s = 7.1$). The mean flow has Mach number 0.5 at the intake ($s = 0$).

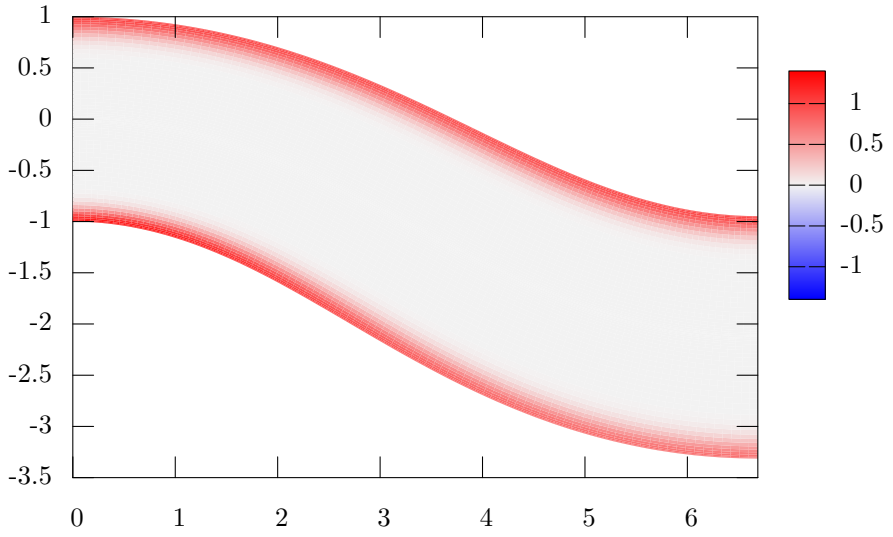

Figure 9. A_0 for the first radial order, 24^{th} azimuthal order mode propagating from the fan face (on the right) to the intake (on the left). The axial wavenumber k for this mode is shown in figure 8 as the lower of the two solid lines.

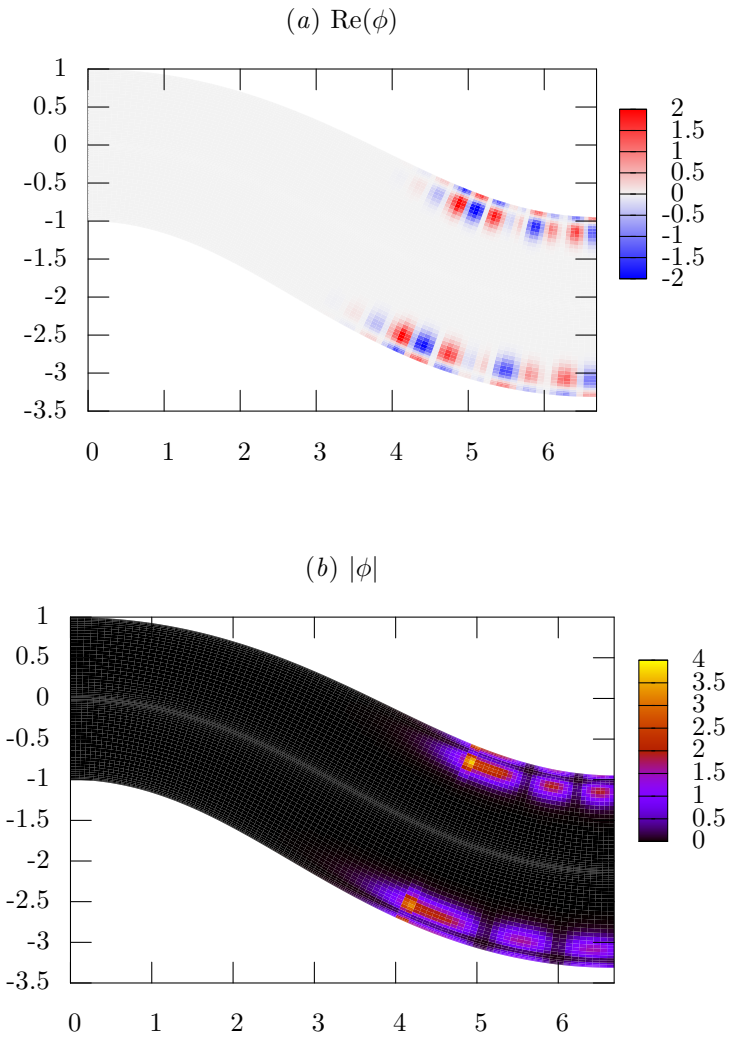

Figure 10. The second radial order, 24^{th} azimuthal order mode propagating from the fan face (on the right) towards the intake (on the left), before being reflected by the duct geometry and propagating back towards the fan face. Consequently, a standing wave is shown at the fan-end of the duct, and an exponentially decaying wave is shown towards the intake end. The axial wavenumbers k for these modes are shown as the upper solid lines in figure 8. (*a*) shows the real part of the wavefunction $\phi = A_0 \exp\{\int \mathrm{i}k(S')/\varepsilon \, \mathrm{d}S'\}$, while (*b*) shows the modulus of the wavefunction $|\phi|$.

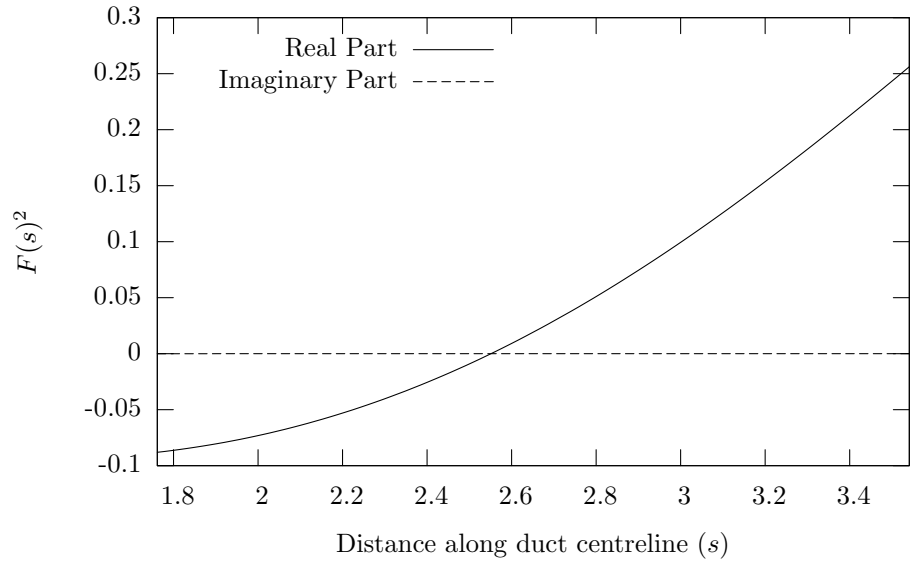

Figure 11. Graph showing the variation of $F(S)^2$ over a cutoff to cuton transition in the RAE 2129 Inlet Diffuser.

Using asymptotic expansions of the Airy function for large $|x|$, see,[24] N has the large-x behaviour

$$\begin{aligned} N &\sim \frac{\mathrm{e}^{\mathrm{i}\pi/4}}{2\sqrt{\pi}x^{1/4}}\left[(A-\mathrm{i}B)\exp\left\{-\frac{4\mathrm{i}}{3}x^{3/2}\right\}-\mathrm{i}(A+\mathrm{i}B)\right] && \text{as } x\to\infty, \\ N &\sim \frac{1}{2\sqrt{\pi}|x|^{1/4}}\left[A+2B\exp\left\{\frac{4}{3}|x|^{3/2}\right\}\right] && \text{as } x\to-\infty. \end{aligned} \tag{12}$$

In order to match with a bounded acoustic field downstream of the turning point it follows immediately that $B = 0$. The second relation in (12) now implies that there is a transmitted cut-off wave in $S > S_0$ and that the transmission coefficient is 1, while the first relation in (12) implies that as well as the incident downstream-going wave there is also an upstream-going reflected wave with reflection coefficient i. This conclusion is exactly the same as is reached for a turning point in a straight duct.[10] This is perhaps surprising, since while the duct curvature over the transition region is constant it is certainly nonzero, so one might have expected curvature-dependent reflection coefficient.

VII. Ray Theory for a hard-walled duct

We will now present some initial work on attempting to find analytically-based approximations for the eigenvalues in our curved duct at high frequency, in the first instance for hard walls. We start off by introducing the ray ansatz for $A_0(r,\theta,S)$ by writing

$$A_0(r,\theta,S) = \frac{\mathcal{A}_0(r,\theta,S)}{\sqrt{h_s D_0}}\exp(-\mathrm{i}\omega\psi(r,\theta,S))\,. \tag{13}$$

We will suppose that ω, the dimensionless frequency, is large so that (13) corresponds to rapidly oscillatory modes, i.e. modes of high order. The corresponding unknown axial eigenvalue, will also be large and so we write $k = \mu\omega$ with $\mu = O(1)$. If we now substitute (13) into (5) and take just the leading terms in ω, i.e. $O(\omega^2)$, we find that

$$(\boldsymbol{\nabla}\psi)^2 = \alpha^2\,, \tag{14}$$

where

$$\alpha^2 = \left[\frac{1}{{C_0}^2} - \frac{2\mu U_0}{h_s {C_0}^2} - \frac{\mu^2}{{h_s}^2}\left(1-\frac{{U_0}^2}{{C_0}^2}\right)\right]. \tag{15}$$

This result is quite important because it shows that, at least as far as determining the allowed values of k is concerned, our problem for the curved duct with variable mean flow can be replaced by considering the modes allowed inside a circular boundary carrying zero mean flow but with spatially-varying sound speed $1/\alpha(r, \theta, S)$. Note that the duct curvature and the duct radii affect α^2 through the mean flow terms (U_0, C_0, and D_0), as well as the curvature appearing in the metric factor h_s. In fact, α^2 only depends on two coordinates, $r\cos\theta$ the transverse position towards the inside or outside of the curve of the duct, and the slow axial coordinate S. The duct modes may therefore be thought of bouncing around inside the cross-section of the duct, being reflected normally by the boundary, subject to a variable wave speed $1/\alpha$ that varies horizontally from the inside to the outside of the bend, but not vertically.

Keller & Rubinow[25] used ray theory to construct a method for determining the eigenvalues of Helmholtz equation in certain closed domains containing a uniform acoustic medium. Their procedure was adapted by Babic & Buldyrev[26] to domains with a varying sound speed. One key step in the Keller & Rubinow procedure is the determination of the shape of a caustic surface inside the domain, which provides an envelope for all possible ray directions. In the case of a circular domain with uniform medium these caustics are simply concentric circles, whose radii are related to be allowed eigenvalues of the problem. However, for a variable sound speed it does not appear possible to determine the shape of this caustic in general, and analytical progress can be made for two particular subsets of all the eigenmodes, termed *bouncing-ball* and *whispering-gallery* modes. Bouncing-ball modes are concentrated about an *extremal ray*, which is a ray that intersects the boundaries at each of its ends at right angles. Not all extremal rays support bouncing-ball modes; to do so, the geometry of the boundary locally about the points of reflection must satisfy a stability condition.[26] Figure 5b shows a bouncing ball mode. Whispering-gallery modes consist of rays running round the perimeter of the boundary, bouncing a large number of times at very short intervals. This is shown schematically in figure 12, and a typical modal shape is shown in figure 5c.

Babic & Buldyrev[26] determined an asymptotic expression for the eigenvalues of whispering-gallery modes of a circle with variable sound speed. These modes are parameterized by two integers: $m \gg 1$, the azimuthal order, and $j = 1, 2, \ldots$, the radial order. For the case of a curved duct, with the effective sound speed given via (15), their analysis gives

$$k_{jm} = \frac{\pi\mu}{I_1(a_2)}\left\{2m + I_2(a_2)\left[\frac{9m}{4I_1(a_2)}\big(j-3/4\big)^2\right]^{1/3}\right\},$$

where

$$\begin{aligned}
I_1(r) &= \int_0^{2\pi} \lambda\, r d\theta,\\
I_2(r) &= \int_0^{2\pi} \lambda^{1/3}\left(\frac{1}{r} + \frac{1}{2\lambda^2}\frac{\partial\lambda^2}{\partial r}\right)^{2/3} r d\theta,\\
\lambda^2 &= \frac{1}{{C_0}^2} - \frac{2\mu U_0}{h_s {C_0}^2} - \frac{\mu^2}{{h_s}^2}\left(1 - \frac{{U_0}^2}{{C_0}^2}\right),\\
\frac{\partial\lambda^2}{\partial r} &= \kappa\cos\theta\left[\frac{(\gamma-1){U_0}^2}{{C_0}^4 h_s} - \frac{2U_0 H(\gamma-1)\mu(2h_s - \mu U_0)}{{C_0}^4 {h_s}^3} - \frac{2\mu^2}{{h_s}^3}\left(1 - \frac{{U_0}^2}{{C_0}^2}\right)\right].
\end{aligned}$$

This expression is valid for both annular and cylindrical ducts; because the rays are bouncing around the outer boundary, the inner boundary plays no part. Note that (VII) gives $k_{jm}(\mu)$ implicitly as a function of $\mu \equiv k_{jm}/\omega$, and an iterative method was therefore used to find the axial wavenumber k_{jm} for a specified value of ω through varying the value of μ. Figure 13 shows the results of the ray tracing asymptotics against numerically calculated eigenvalues. A frequency of $\omega = 40$ was used for the comparison, so as to allow high azimuthal order modes to be cuton. The results are plotted against the azimuthal order m so the individual modes can be distinguished. The agreement is seen to be reasonable, especially for nearly-cutoff large-m modes, as is to be expected from using large m asymptotics.

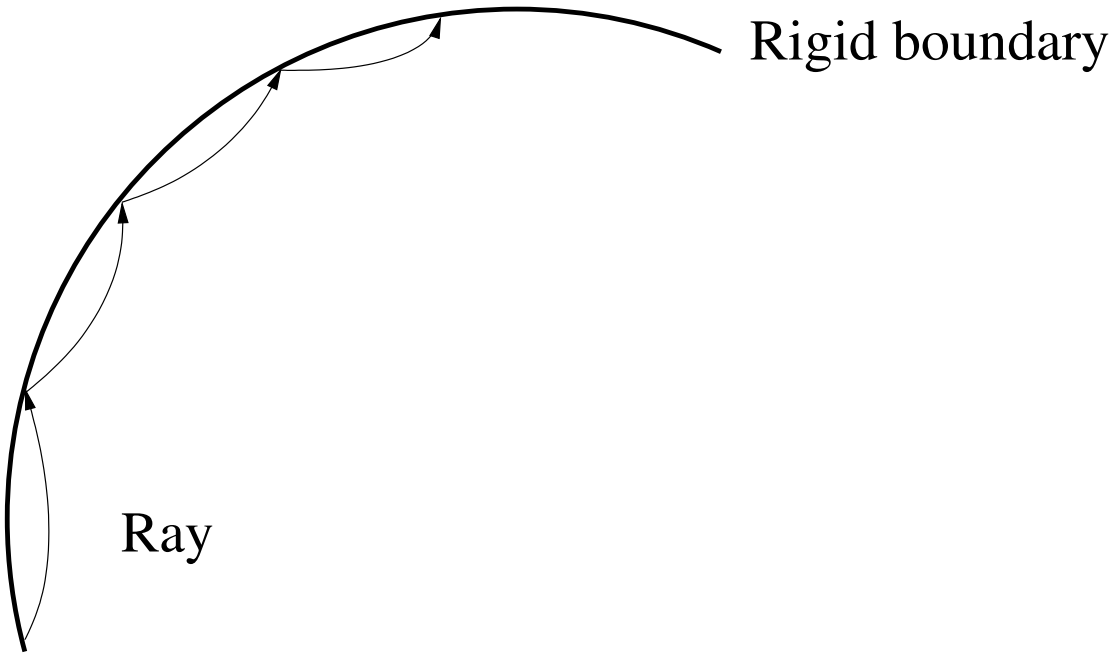

Figure 12. Schematic diagram of the rays for a whispering-gallery mode; the rays are reflected with incidence angle equal to reflection angle, and are then refracted by the spatially nonuniform effective sound speed.

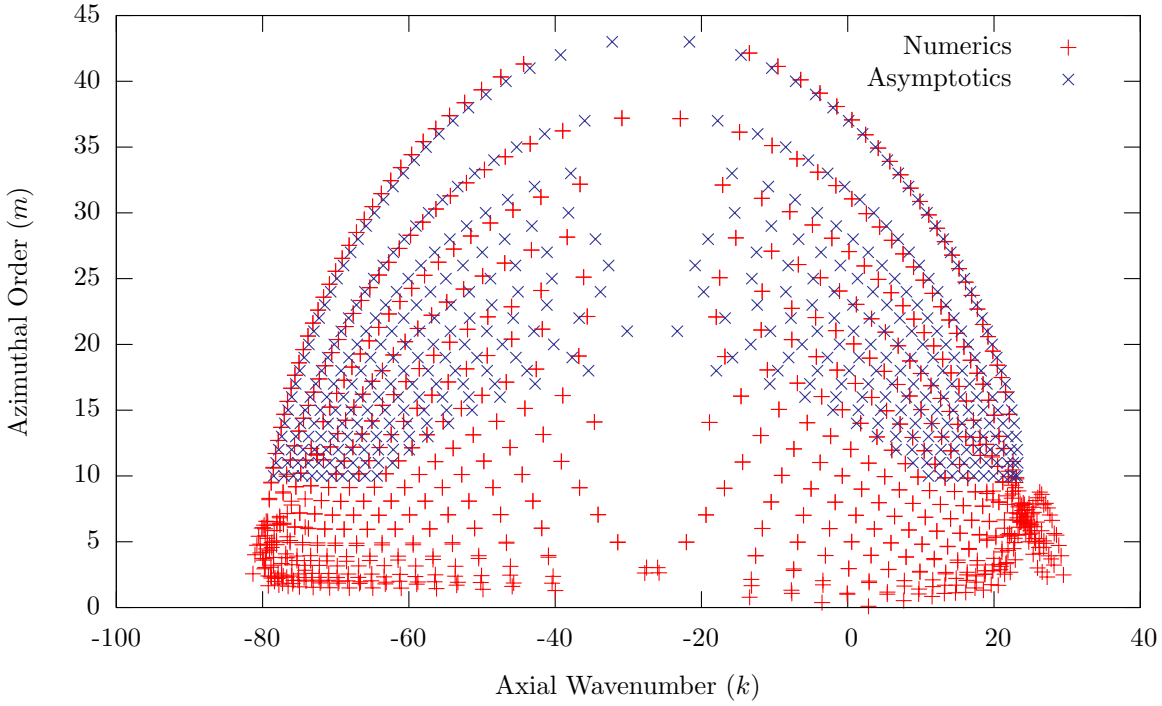

Figure 13. Comparison of ray tracing asymptotics against numerical results. The azimuthal order for the numerics was estimated using a Fourier transform and averaging. $U_\infty = 0.5$, $\kappa = 0.1$, and $\omega = 40$.

VIII. Concluding Remarks

In this paper we have considered the propagation of acoustic waves along a curved duct carrying mean potential flow. The curvature of the duct centreline and the wall radii have been assumed to vary slowly along the axis, allowing application of an asymptotic multiple scales analysis. We have seen that the spectrum of local eigenmodes is more complicated than in the straight-duct case, due to the fundamental asymmetry between upstream and downstream propagating modes, with some mode shapes tending to be concentrated on either the inside or outside of the bend depending on the direction of propagation. Our closed-form expression for the variation of the slowly-varying amplitude is very similar in form to the straight-duct case, however, and describes the balance between energy flux along the duct and dissipation by the (lined) walls.

The work presented in this paper is being extended in a number of ways. First, the restriction that the duct centreline is planar can be relaxed. This means that as well as a nonzero slowly-varying curvature the duct centreline will possess a slowly-varying torsion $\tau(S)$. Germano[27] shows how the coordinate system can be modified to account for this effect, simply by replacing the cross-sectional polar angle θ by

$$\theta + \frac{1}{\epsilon}\int_0^S \tau(S')\mathrm{d}S' \,, \tag{16}$$

which yields an orthogonal coordinate system which effectively twists with the duct centreline. The one difficultly with $\tau \neq 0$, however, is that the mean flow becomes much more complicated with the cross-sectional components V, W becoming $O(1)$ rather than $O(\epsilon)$ when $\tau = 0$. (Of course, in the absence of mean flow the transformation (16) can be straightforwardly applied to the methodology of the present paper to yield a solution for nonzero torsion.)

Second, the pseudo-spectral eigenvalue solver is sufficiently general to allow straightforward extension of our solution to more complicated geometries. Two cases in particular include the case of lining only half the duct circumference, and the curved-duct version of Rienstra's solution[12] for an arbitrary cross-section. Third, we are interested in the case in which larger amplitude disturbances propagate along the duct, and we are therefore at present completing a weakly nonlinear version of the analysis presented here.

Acknowledgements

This work has been supported by an EPSRC CASE award from Rolls-Royce. Helpful discussions with Dr SW Rienstra are gratefully acknowledged.

References

[1]Keefe, D. and Benade, A., "Wave propagation in strongly curved ducts," *J. Acoust. Soc. Am.*, Vol. 74, 1983, pp. 320–332.

[2]Pagneux, V., Amir, N., and Kergomard, J., "A study of wave propagation in varying cross-section waveguides by modal decomposition. Part I. Theory and validation," *J. Acoust. Soc. Am.*, Vol. 100, 1996, pp. 2034–2048.

[3]Pagneux, V., Amir, N., and Kergomard, J., "A study of wave propagation in varying cross-section waveguides by modal decomposition. Part II. Results," *J. Acoust. Soc. Am.*, Vol. 101, 1996, pp. 2504–2517.

[4]Felix, S. and Pagneux, V., "Sound propagation in rigid bends: A multimodal approach," *J. Acoust. Soc. Am.*, Vol. 110, 2001, pp. 1329–1337.

[5]Felix, S. and Pagneux, V., "Mulitmodal analysis of acoustic propagation in three-dimensional bends," *Wave Motion*, Vol. 36, 2002, pp. 157–168.

[6]Felix, S. and Pagneux, V., "Sound attenuation in lined bends," *J. Acoust. Soc. Am.*, Vol. 116, 2004, pp. 1921–1931.

[7]Ting, L. and Miksis, M., "Wave propagation through a slender curved tube," *J. Acoust. Soc. Am.*, Vol. 74, 1983, pp. 631–639.

[8]Gridin, D. and Craster, R., "Quasi-modes of a weakly curved waveguide," *Proc. Roy. Soc. Lond. A*, Vol. 459, 2003, pp. 2909–2931.

[9]Adamou, A., Gridin, D., and Craster, R., "Acoustic quasi-modes in slowly varying cylindrical tubes," *Q. J. Mech. Appl. Math.*, Vol. 58, 2005, pp. 419–438.

[10]Rienstra, S. W., "Sound Transmission in Slowly Varying Circular and Annular Lined Ducts with Flow," *J. Fluid Mech.*, Vol. 380, 1999, pp. 279–296.

[11]Rienstra, S. W. and Eversman, W., "A Numerical Comparison Between the Multiple-Scales and Finite-Element Solution for Sound Propagation in Lined Flow Ducts," *J. Fluid Mech.*, Vol. 437, 2001, pp. 367–384.

[12]Rienstra, S. W., "Sound Propagation in Slowly Varying Lined Flow Ducts of Arbitrary Cross-Section," *J. Fluid Mech.*, Vol. 495, 2003, pp. 157–173.

[13]Cooper, A. J. and Peake, N., "Propagation of Unsteady Disturbances in a Slowly Varying Duct with Mean Swirling Flow," *J. Fluid Mech.*, Vol. 445, 2001, pp. 207–234.

[14]Ovenden, N., "A uniformly valid multiple scales solution for cut-on cut-off transition of sound in flow ducts," *J. Sound Vib.*, Vol. 286, 2004, pp. 403–416.

[15]Menzies, R. D. D., *Investigation of S-Shaped Intake Aerodynamics using Computational Fluid Dynamics*, Ph.D. thesis, University of Glasgow, 2002.

[16]Goldstein, M. E., "Unsteady Vortical and Entropic Distortions of Potential Flows Round Arbitrary Obstacles," *J. Fluid Mech.*, Vol. 89, 1978, pp. 433–468.

[17]Myers, M. K., "On the Acoustic Boundary Condition in the Presence of Flow," *J. Sound Vib.*, Vol. 71, No. 3, 1980, pp. 429–434.

[18]Hinch, E., *Perturbation Methods*, Cambridge, 1991.

[19]Khorrami, M. R., Malik, M. R., and Ash, R. L., "Application of Spectral Collocation Techniques to the Stability of Swirling Flows," *J. Comput. Phys.*, Vol. 81, 1989, pp. 206–229.

[20]Boyd, J. P., *Chebyshev and Fourier Spectral Methods, Second Edition*, Dover, 2001.

[21]Rienstra, S. W., "A Classification of Duct Modes based on Surface Waves," *Wave Motion*, Vol. 37, 2003, pp. 119–135.

[22]Brambley, E. J. and Peake, N., "Classification of Aeroacoustically Relevant Surface Modes in Cylindrical Lined Ducts," *Wave Motion*, Vol. 43, 2006, pp. 301–310.

[23]Cooper, A. J. and Peake, N., "Trapped acoustic modes in aeroengine intakes with swirling Flow," *J. Fluid Mech.*, Vol. 419, 2000, pp. 151–175.

[24]Abramowitz, M. and Stegun, I. A., *Handbook of Mathematical Functions*, Dover, 1974.

[25]Keller, J. B. and Rubinow, S. I., "Asymptotic Solution of Eigenvalue Problems," *Annals Phys.*, Vol. 9, 1960, pp. 24–75.

[26]Babic, V. M. and Buldyrev, V. S., *Short-Wavelength Diffraction Theory*, Springer, 1991.

[27]Germano, M., "On the effect of torsion on a helical pipe flow," *J. Fluid Mech.*, Vol. 125, 1982, pp. 1–8.